Eurographics Workshop on Visual Computing for Biology and Medicine (2019)
B. Kozlíková, L. Linsen, and P.-P. Vázquez (Editors)

Pelvis Runner: Visualizing Pelvic Organ Variability in a Cohort of Radiotherapy Patients

N. Grossmann[1], O. Casares-Magaz[2], L.P. Muren[2], V. Moiseenko[3], J.P. Einck[3], M.E. Gröller[1,4], R.G. Raidou[1]

[1]TU Wien, Austria, [2]Department of Medical Physics, Århus University Hospital, Denmark
[3]Department of Radiation Medicine and Applied Sciences, UC San Diego, United States, [4]VRVis Research Center, Austria

Abstract

In radiation therapy, anatomical changes in the patient might lead to deviations between the planned and delivered dose—including inadequate tumor coverage, and overradiation of healthy tissues. Exploring and analyzing anatomical changes throughout the entire treatment period can help clinical researchers to design appropriate treatment strategies, while identifying patients that are more prone to radiation-induced toxicity. We present the Pelvis Runner*, a novel application for exploring the variability of segmented pelvic organs in multiple patients, across the entire radiation therapy treatment process. Our application addresses (i) the global exploration and analysis of pelvic organ shape variability in an abstracted tabular view and (ii) the local exploration and analysis thereof in anatomical 2D/3D views, where comparative and ensemble visualizations are integrated. The workflow is based on available retrospective cohort data, which incorporate segmentations of the bladder, the prostate, and the rectum through the entire radiation therapy process. The* Pelvis Runner *is applied to four usage scenarios, which were conducted with two clinical researchers, i.e., medical physicists. Our application provides clinical researchers with promising support in demonstrating the significance of treatment plan adaptation to anatomical changes.*

CCS Concepts
• ***Human-centered computing*** → ***Visual analytics;*** • ***Applied computing*** → ***Life and medical sciences;***

1. Introduction

Prostate cancer is the most frequent type of cancer among men [DJFB05]. Radiation therapy is a common therapeutic approach against it, requiring detailed treatment planning to identify where the tumour is located and to calculate how to treat it effectively [WL15]. In radiation therapy, high radiation doses are administered to "destroy" the tumor. However, apart from the tumor, also the surrounding healthy tissue may be affected by radiation, leading to potentially severe side effects—commonly known as *toxicity*. Modern treatment techniques allow for a more precise treatment, but toxicity remains a problem for a number of patients [CMMH*17, MLK*07, VYM*10].

Recent clinical research suggests that anatomical variability of certain patients can lead to increased radiation doses being delivered to healthy organs, such as the bladder or the rectum [CMMH*17]. The main reason is that the dose is delivered in multiple sessions over a period of weeks, when the natural anatomical variations of the organs may cause deviations between planned and delivered doses. During these sessions, alignment corrections are made before dose administration, but the the main goal of alignment is to ensure that the tumor is positioned correctly. In *adaptive radiotherapy*, adapting the workflow to encompass changes in organ shape is anticipated to enable higher precision with less damage to healthy tissues [THLM*13].

To achieve this, clinical researchers, such as medical physicists, working on the design of robust treatment strategies require a better understanding of the general shape and position variability of all pelvic organs, as well as the anatomical variability of subgroups of patients [CvHvdK*11, LvHB*05, CvHHB12, RDCO*17]. To evaluate the overall robustness of specific treatment options, cohort analysis is conducted in retrospective studies, while individual patient or cohort partition exploration accounts for particular cases. This has been proposed in the past only for the case of the bladder [RCMA*18, CMRP*19, CMMH*17], but radiotherapy treatment involves a number of other organs, as well. By providing an application to estimate and visualize the shape variability of pelvic organs, we aim to support clinical researchers in demonstrating the significance of dose plan adaptation to anatomical changes.

The contribution of this work is the design and development of a novel application, the *Pelvis Runner*. The *Pelvis Runner* is to be used by clinical researchers for the exploration of a cohort of pelvic organs segmented from multiple patients, across the whole radiation treatment procedure. We focus on the *global exploration and analysis of the shape variability of all pelvic organs in a cohort of patients* **(T1)** and on the *local exploration and analysis of all pelvic organs in individual patients or cohort partitions* **(T2)**.

The *Pelvis Runner* builds upon the previous work of the *Bladder Runner* [RCMA*18]—an application for the detailed visual ex-

DOI: 10.2312/vcbm.20191233

ploration and analysis of the impact of bladder shape variation on the accuracy of dose delivery, during the course of prostate cancer radiotherapy. For the *Pelvis Runner*, we retrospectively employed pelvic organ data from a cohort of 24 prostate cancer patients, for whom detailed CT data were available for 13 treatment sessions. The current application allows clinical researchers to explore the entire pelvis anatomy of a large cohort of patients in a quick and easy way, and also enables in-depth exploration of particular patients or partitions of the cohort.

2. Clinical Background

For patients diagnosed with prostate cancer, a common treatment method is external beam radiotherapy (EBRT). EBRT follows a complex workflow, which involves an interdisciplinary team and incorporates several processes from imaging to pre-processing, and from treatment plan simulation to evaluation [SRM*19]. Radiation doses are delivered using multiple beams aimed at the tumor location. When superimposed, these beams sum up to a high dose applied to the targeted tumor area and a lower dose to the surrounding tissue. The planned dose is not administered at once, but is instead split up over several weeks, to allow the recovery of healthy tissue, while minimizing tumor growth [WL15]. This is called *fractionation*, and its distinct sessions are called *fractions*. Recent techniques allow us to effectively spare normal tissue, while delivering the desired high dose to the tumor volume [QLL*12]. However, parts of healthy organs of the pelvis are still unavoidably irradiated and this can lead to side-effects affecting the quality of life of the patient. This is referred to as *radiation-induced toxicity*.

The anatomy of the male pelvis is depicted in Figure 1. In every human, it presents unique variations, which can be naturally occurring across individuals, occurring due to pathological factors, or due to day-to-day changes in the same person. The latter occurs because the pelvic organs consist of soft deformable tissues, which are flexible and their shapes are affected by filling changes [MSD03, CvHvdK*11, LvHB*05, CvHHB12, RDCO*17]. Organs, such as the bladder and the rectum, whose position and shape varies significantly, are especially prone to this effect [VYM*10]. Recent works suggest a link between pelvic organ motion and deformation, and increased toxicity risks [CMMH*17]. This is due to the inherent complexity of the radiation therapy workflow, which does not make it possible to adapt the treatment plan before every fraction. Usually, tumor location is prioritized.

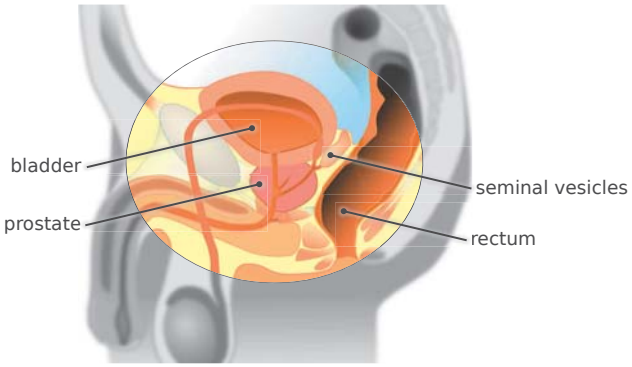

Figure 1: *Pelvic organs of the male body. We depict the main organs included in the* Pelvis Runner.

The standard treatment procedure is to generate one initial treatment plan and to use it as a basis for all subsequent sessions. To facilitate this, the setting of the initial planning is reproduced during the treatment. For example, prostate treatment commonly requires a full bladder regime [WL15], while positioning inaccuracies are addressed with simple translational adaptations. As there are many different factors that lead to shape deformations and position variations over the course of the treatment, these cannot be entirely covered by these small adaptations to the initial plan [CMMH*17]. The necessity for a more drastic adjustment of the target volume in prostate cancer therapy on a per-treatment basis has been highlighted by several recent works [VYM*10, CvHvdK*11, LvHB*05, CvHHB12, RDCO*17]. Prostate cancer research starts looking into adaptive treatment approaches—similarly to lung cancer treatment where breathing motion is considered—that will take into account the shape variability and movement of the pelvic organs of the patient through treatment [THLM*13].

In clinical practice, the evaluation of a treatment plan is currently done in two ways [SRM*19]. Both approaches are shown in Figure 2. First, spatial 2D/3D views allow the experts to see how the dose affects the tumor and its surrounding organs for a given point in the treatment period [NDSM*19]. This approach does not allow for an easy exploration of multiple patients at the same time—an important tool for judging the robustness of treatment strategies, which is often done in retrospective studies. Second, dose volume histograms (DVHs) show how much radiation is received by the volume of each organ and allow the experts to quickly identify organs at risk of toxicity [WL15]. Although DVHs scale well for a large number of patients, they do not allow for an easy link to patient anatomy. Adequate tools for the inspection and analysis of pelvic organ variability within the content of radiotherapy do not exist—with the exception of the *Bladder Runner* [RCMA*18]. This application has demonstrated its clinical usefulness in a retrospective clinical study with a single focus on bladder toxicity in cohorts of patients [CMRP*19]. However, the *Bladder Runner* does not support the exploration of anatomical variability of *all pelvic organs* during the entire radiotherapy treatment period. It also does not support the exploration of *motion* of the pelvic organs.

Employed Dataset: For this work, we had access to data from a cohort of 24 patients undergoing radiation therapy for prostate cancer. The provided data includes 13 treatment sessions, for each pa-

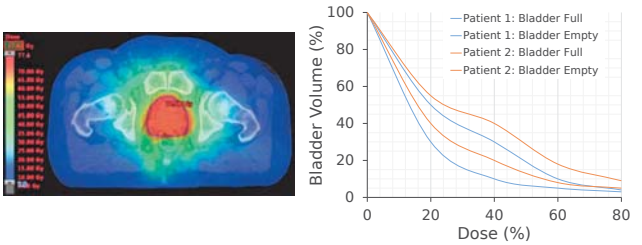

Figure 2: ***Left:*** *Spatial 2D view on the radiation therapy plan of one patient.* ***Right:*** *Dose Volume Histogram of two patients for two treatment regimes (empty and full bladder).*

tient. The first five are from the five daily sessions of the first week, while the subsequent datasets were evenly sampled from the following treatment weeks [CMMH*17]. The initial treatment plan was calculated for patients with an empty rectum and full bladder. At each session of their treatment, the patients were instructed to have roughly the same organ fillings. Before each treatment, a Cone Beam Computed Tomography (CBCT) acquisition was done for patient alignment using rigid translations. For each of these sessions, we were provided with pelvic organ delineations in the form of contour lines. For all patients, the bladder and rectum delineations are available. Additionally, the patient data might incorporate delineations of either the prostate, or the prostate and seminal vesicles, or the prostate, seminal vesicles and lymph nodes. Within the context of this work, we use for simplicity the term "prostate" for the first category (prostate only) and "clinical target volume or CTV" for the other two. The dataset is depicted in Figure 3.

3. Related Work

To facilitate understanding of the daily occurring shape variations in pelvic organs and especially their correlation to toxicity, some works have already been performed by clinical experts [NDSM*19, CMMH*17]. These are, however, limited to the exploration of spatial 2D/3D views or DVH analysis, as discussed in the previous section. These works give insight into what kind of visualizations are common to clinical experts, and also show that looking at more than one patient or more than one time point of treatment simultaneously is a tedious process that does not scale well. Solutions for the visualization of many pelvic organs in an entire cohort of patients through the entire treatment period can be provided by the domains of *shape space* and *cohort analysis*, and in *comparative and ensemble visualization*.

Our *Pelvis Runner* is building upon the previous work of the *Bladder Runner* [RCMA*18]. The *Bladder Runners* aims at providing information about the amount of irradiation applied to the bladder across the treatment for a cohort of patients. The entire approach is based on a 14D shape descriptor vector for the cohort of bladders [PI97]. The 14D shape descriptors are given as input to a t-Distributed Stochastic Neighbor Embedding (t-SNE) [MH08] followed by clustering [CM02] to detect cohort partitions with similar bladder shapes and evolutions through the treatment period. Using multiple coordinated views, the clinical experts are enabled to

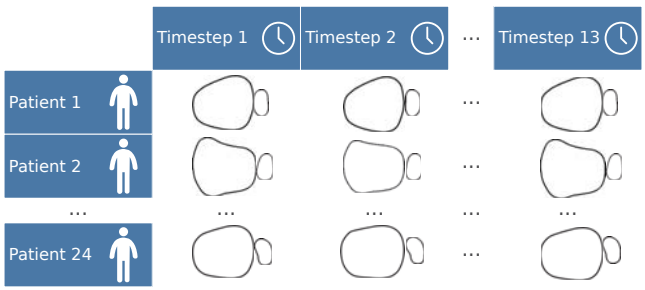

Figure 3: *Schematic depiction of the cohort data used in this work. The delineations of pelvic organs of 24 patients are available, with each of them having 13 sessions throughout their treatment. For each patient, multiple organs are delineated.*

analyze the cohort of bladders through the radiotherapy treatment sessions, while the dose distributions and toxicity information are also incorporated in the views. We are hereby extending the application to multiple organs, including the possibility of having different subsets of organs in the data (e.g., for one patient we have the delineations of the bladder, rectum and prostate and for another one we have additionally the seminal vesicles).

Other previously proposed frameworks include the work of Reiter et al. [RBGR18], who are able to explore and analyze the variability in multiple pelvic organs. For this, they use an approach based on spherical harmonics [KFR03]. To distinguish clusters across organ classes, they employ t-SNE [MH08], while to distinguish clusters within organ classes (and more importantly, outliers) they use Principal Component Analysis (PCA) [Shl14]. Yet, this approach does not support multi-timepoint analysis, while their data is derived from automatic segmentation algorithms where a triangle-to-triangle correspondence can be ensured across the individual structures. Generally, the use of descriptors, as presented in the former works, supports the efficient differentiation between different shapes, but it lacks the ability to synthesize arbitrary elements in their shapes.

In *shape space analysis*, Hermann et al. [HSK11, HSSK14, HSSK16] investigate anatomic covariances in ensembles of data, providing also a state of the art report with future prospects on the visual analysis of shapes [HK15]. Busking et al. [BBP10] propose to use a 2D scatter plot to represent the distribution of elements inside a cohort and to synthesize additional arbitrary objects in the shape space. For comparing objects, they later deal with visualizing intersecting 3D surface meshes [BBF*11]. Landesberger et al. [VLBK*13] extend the scatter plot concept for parameter sensitivity analysis in segmentation and the link to the segmentation outcomes. Considering the high learning curve for many complex visualizations of high dimensional data, such as cohort data, Blumenschein et al. [BBS*18] propose visualization concepts aimed at people who are not necessarily visualization-literate.

More specifically for *cohort analysis*, Klemm et al. [KLR*13] focus on the extraction of spine canal variability and the exploration of clusters of similarly shaped spines. This work has been extended to incorporate additional patient information [KOJL*14], demonstrating how to effectively reduce and visualize image cohort data and to facilitate their understanding on a broader basis. Steenwijk et al. [SMB*10] also go beyond shape analysis by proposing a framework for the interactive and structured visual analysis of cohort data. Cohort analysis has also been tackled by Preim et al. [PKH*16], Bernard et al. [BSM*15] and Alemzadeh et al. [AHN*17], for various purposes.

Given the available data, which are contour delineations of the pelvic organs, we cannot overlook the previous work in *ensemble visualization* [WHLS18]. Our work relates to contour boxplots by Whitaker et al. [WMK13], their extension for streamline ensemble data by Mirzargar et al. [MWK14], and the recent techniques of Ferstl et al. [FBW16, FKRW16, FKRW17]. The latter are applied on weather simulation ensemble data, covering 2D lines, 3D volumes and also the time evolution thereof. In *comparative visualization* [KCK17], for the investigation of jaw movement, Keefe et al. [KERC09] introduce small juxtaposed representations, where

the movement is explicitly encoded giving a good overview of all the data, while parallel coordinates allow for an in-depth search. Tory et al. [TMA01] investigate a superposition approach for the development of brain lesions extracted at different time points from MRI images. The use of explicit encoding to highlight structural differences is used by Schmidt et al. [SPA*14], where they can compare a large number of similar meshes and can quickly identify regions of differences in multiple linked views.

To sum up, previous literature includes several approaches that are able to tackle a multitude of individual objects (in our case, either multiple patients or multiple organs)—possibly, even different object sets, i.e., missing some instances (organs). Also, previous work proposes approaches that visualize the development of structures through time (in our case, multiple timesteps). The most relevant works and their characteristics are represented in Table 1, showing that an approach that encapsulates all these aspects is not available yet. We aim to cover this gap with the *Pelvis Runner*.

4. Method

The *Pelvis Runner* focuses on two main objectives: the *global exploration and analysis of all pelvic organs shape variability across the treatment period and across a cohort of patients* **(T1)** and the *local exploration and analysis of all pelvic organs shape variability across treatment period for individual patients* **(T2)**. Clinical researchers are initially interested in extracting the *amount of variability* of the available pelvic organs among all patients and across time. We, therefore, need to calculate a *simple descriptor* for each individual organ class that allows us to quantify organ similarity and estimate the variability of each organ. Subsequently, we need to visualize the variability of the organ classes within the *whole cohort*. This provides a quick overview on the entire cohort, as well as capabilities to identify patients or organs with high variability, i.e., outliers. At this point, patient and time correspondences should not be lost. When interesting parts of the cohort are identified, a more *detailed exploration* needs to be conducted. Drilling down to individual objects should be possible, i.e., exploring individual patients or individual organs, to understand which regions of certain organs are prone to variations and how large these differences are. Changes in position and in shape should be both displayed.

Table 1: *Schematic depiction of the most relevant previous work and which main aspects of our application they fulfill.*

	Multiple Organs	Possibly Different Organ Sets	Multiple Patients	Multiple Timepoints
Raidou et al. [RCMA+18]	×	×	✓	✓
Reiter et al. [RBGR18]	✓	×	✓	×
Hermann et al. [HSK11, HSSK14, HK15]	×	×	✓	×
Busking et al. [BBP10]	×	×	✓	×
Landesberger et al. [VLBK+13]	×	×	✓	×
Blumenschein et al. [BBS+18]	×	✓	✓	×
Klemm et al. [KLR+13, KOJL+14]	×	×	✓	×
Steenwijk et al. [SMB+10]	×	×	✓	×
Mirzagar et al. [MWK14]	×	×	✓	×
Ferstl et al. [FBW16, FKRW16, FKRW17]	×	×	✓	✓ [in FKRW17]
Keefe et al. [KERC09]	×	×	✓	✓
Tory et al. [TMA01]	×	×	×	✓
Schmidt et al. [SPA+14]	×	×	✓	×

Our general workflow is presented in Figure 4. Our approach starts with data processing, and with quantifying the similarity of the volumetric organ shapes of the organs in order to estimate their variability. For visualizing the variability in the organ shapes, an aggregation approach based on Ferstl et al. [FKRW16] is employed. For **(T1)**, a low dimensional embedding of each organ is used to calculate the variability on a per-patient basis and to visualize the whole cohort. After clustering, a tabular plot is employed to explore the cohort partitioning in a flexible and intuitive manner. For **(T2)**, information on the anatomical space is shown on demand. We enable the user to drill down to selected groups or patients from the cohort and to perform a detailed inspection of the organ variations. This is achieved by reconstructing the initial 3D objects from their low dimensional embeddings. By sampling the embedding space for the median and the standard deviations, we reconstruct the shape variations and we show them in a representation similar to contour boxplots [WMK13].

4.1. Data Processing, Shape Analysis and Display

The first step in the shape analysis is to *transform* the data into a format that is easier to handle and to visualize. We use a combination of volumetric data and triangular meshes, generated from the available contour data. The volumetric data allows us to directly analyze the data and to perform further calculations. However, while the calculations are easier in this space, the visualization is computationally more expensive. Thus, for the visualization components, we employ the triangular meshes.

For the *registration*, we retain all organs of every individual patient at their relative positions and we only align patients to each other. We do so, by estimating the mean center of all organ positions across time. Although this approach adds small translational variations, it preserves the volume changes and their main growth directions, which is our main focus in this work.

Furthermore, we need to *reduce* our 3D volumetric patient data into a low dimensional vector representation that can be employed for the statistical analysis of the cohort. At the same time, we need to map the two dimensions of our cohort, i.e., patients and timesteps, into a single one without losing correspondences within the data. For this, we employ linearization strategies along two curve types: Scanline Curve and Hilbert Curve [Hil35]. The former approach is employed to unravel the individual patients and timesteps, as we are interested in preserving the temporal order

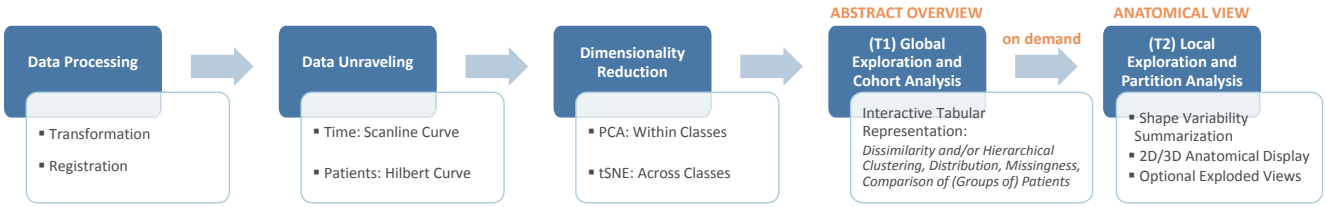

Figure 4: *Schematic depiction of the workflow and the main components of* Pelvis Runner.

within the data. In this way, we can create a vector where all timesteps of the first patient are followed by the timesteps of the second patient, and so forth. This allows us to easily select patients and their timesteps, while we can also efficiently add new patients in the analysis. For the unfolding of the 3D volumetric data, we select a Hilbert Curve approach that allows us to analyze how the shape differentiation capabilities of our method changes if the sampling density is reduced. This has also been employed in the work of Weissenböck et al. [WFG*19] for volume data comparison.

After the volumetric data are transformed into vectors without losing patient and timestep correspondence within the cohort, they are *displayed*. For this, we create a low dimensional embedding, which allows us to create a computationally efficient way to store and process large cohorts of patient data. The dimensionality reduction step creates a low dimensional representation of the structure of the high dimensional space where each cohort datapoint, i.e., individual patient organ at a specific timestep, is represented by one position in space, where similar shapes are placed nearby. We employ a Principal Component Analysis (PCA) [Shl14], when we are more interested in the differentiation within classes of organs. We combine it with a t-Distributed Stochastic Neighborhood Embedding (t-SNE) [MH08], when we are more interested in the differentiation across organ classes, as in Reiter et al. [RBGR18].

4.2. (T1) Global Exploration and Analysis of a Cohort

For the global exploration and analysis of the entire cohort, we need to enable clinical researches to manage the comparison of the *different pelvic organs* in *multiple patients* throughout *several timesteps*. Additionally, the patient data might incorporate *different sets of organs*, as the delineations include either the prostate, or the prostate and seminal vesicles, or the prostate, vesicles and lymphs.

We first provide users with an *overview of the whole cohort data*. The main idea behind this is to generate a high-level representation that conveys the general patterns present in the data, before the user starts a detailed investigation of individual interesting cases. This is based on the low dimensional outcome of the previously discussed dimensionality reduction step. The distance calculation between datapoints enables the explicit estimation of outliers on a per-patient basis, if the distance to their mean shape is used. It also gives an indication on how much the shape varies across the treatment timepoints for each patient. For this, we calculate the *Euclidean distance*, similar to Klemm et al. [KLR*13]. If clustering would be employed for this task instead, subtle differences would not be visible. Clustering would only offer a binary variability option—either the shape belongs to a cluster or not. On the other hand, clustering enables the extraction of the main shape groups within patients. These can be later analyzed and compared to one another, offering an understanding on what shape types are to be expected and how prominent they are. As both subtasks are valid, the user can deploy both options in the application. For the clustering, we employ a *hierachical clustering with complete linkage* [ELL01].

From the previous calculations, we receive a single distance metric and/or cluster value per combination of patient, timestep and organ. To represent this, we employ a *tabular representation* similar to the contingency matrix of the *Bladder Runner* [RCMA*18] or the representation in the work of Blumenschein et al. [BBS*18]. This representation (Figure 5) was chosen to show the shape change information, while at the same time preserving information about time and patient correspondences. We also want to ensure that the visualization itself is readily understandable by users who do not employ visual analytics tools on a regular basis. In the tabular view, patients are denoted on the vertical axis and timesteps on the horizontal one, to enable comparison both across timesteps and patients. The encoded values may represent the similarity distance encoded with a sequential white(low)-to-blue(high) colormap (Figure 5), or cluster membership denoted with a qualitative colormap (Figure 10 (a)). Both of these maps were taken from Colorbrewer [HB03]. To extend this approach for multiple organs, we split each cell of the tabular view into equally sized parts—one for each organ to be shown (Figure 5, right). With this encoding, the users can directly compare values of multiple organs and detect patterns and correlations, similar to a glyph-based representation, as also demonstrated by Blumenschein et al. [BBS*18]. The users can manually filter which organs are shown at any given time, as well as whether they want to show the Euclidean distance or the clustering. Labels and legends accompany the representation.

The tabular representation can accommodate additional information with regard to the *underlying data distribution* and to the amount of *missing data*, i.e., missing organ delineations, as both of these indicate trustworthiness. The former is represented with additional distribution histograms accompanying the groups and positioned to the left-hand side of the tabular plots, as shown with the grey bars in Figure 5. The latter is represented with an "empty glass" metaphor on each cell in the tabular plot. As shown in Figure 6 (left), the emptier the cell, the less data it contains and this partition is less trustworthy. For example, in Figure 6 (left), Groups 1 and 2 have less available data for the prostate (third component of the glyph, see also legend) than Group 3. Going one step further, the user might also be interested in finding out how different *shape group types compare* to each other. For this, several encodings, i.e., size, texture, color, and blur, have been investigated, as shown in Figure 6 (right), for the encoding of the standard deviation of each observation from the mean value.

While the initial layout of the overview visualization provides

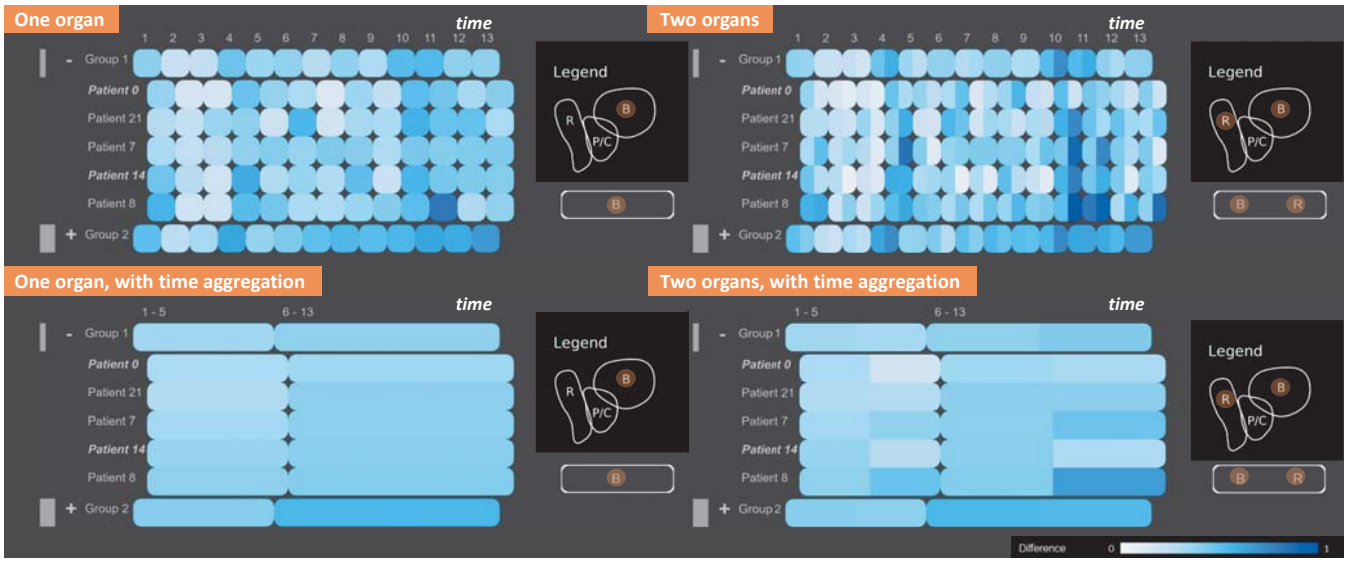

Figure 5: *Some of the possible configurations of the tabular view—with one or multiple organs, and with or without time aggregation.*

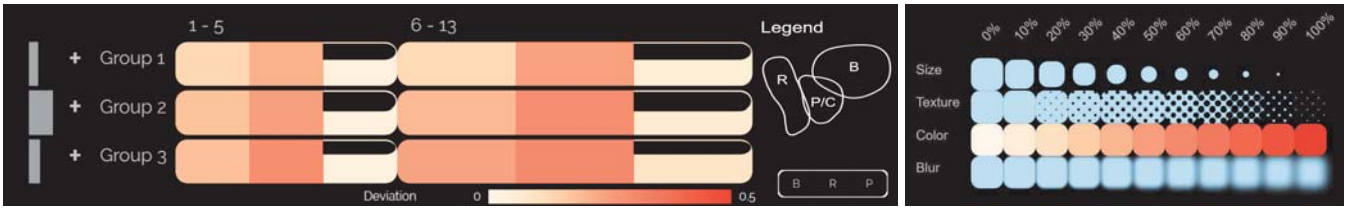

Figure 6: ***Left:*** *Encodings for the standard deviation from the mean shape (orange colormap) and for data missingness (emptiness of cells).* ***Right:*** *Alternative encodings for the standard deviation of each organ from the mean value (size, texture, color, and blur).*

clinical researchers with the option to see the whole cohort at once, the analysis process would require the user to scan row-by-row the representation to detect similarities or outliers. This can be time-consuming even for a small cohort of patients. To this end, we additionally enable Focus+Context (F+C) [BCS96], sorting and filtering [FGS*17], visual aggregations, e.g., based on significant time-points as shown in the bottom row of Figure 5, and additional partitioning based on patient metadata, e.g., available retrospective toxicity data.

4.3. (T2) Local Exploration and Analysis of Partitions

During the exploration and analysis of the entire cohort, the users identify specific interesting cases, i.e., individual patients or partitions of the cohort, which require further investigation. We enable the users to drill down to individual patients or partitions, for local exploration. Up to this point, only abstract key figures with regard to the cohort and its shape properties have been displayed in the tabular view. We provide an additional view on the anatomical shape of selected patients or partitions. Multiple patients or subgroups within the cohort are selected respectively by clicking on a cell or a row label in the cohort visualization. Each selection gets assigned a unique color from a qualitative scheme by Colorbrewer [HB03].

For the *summarization of shape variations*, we extract the median element inside the shape space as a general representative of the group. In this way, we are able to retrieve a representative shape that exists in our cohort—as opposed to the mean shape. The analysis of the center point variations is indicative of the organ movement. For this, we also use the mean and standard deviation of the center point of each organ to calculate the main variation directions for groups of organs. This is also in accordance with our used registration method, where we also took the average center point for each patient to align its organs before the analysis. Before this step, we have already performed a Kolmogorov-Smirnoff test to confirm that the distribution of the shapes within the cohort is indeed close to a normal distribution. This combined approach has also been employed by Ferstl et al. [FBW16, FKRW16].

To *display the above summarized shape and position variability*, we employ the common combination of three anatomical 2D planes (sagittal, coronal and axial) with a 3D view, e.g., in Figure 9 (c). Standard interaction, e.g., zooming, panning, slicing through the volume, is possible. For the comparative visualization [KCK17] of the pelvic organs of multiple patients within a 2D view, two alternatives are possible: (i) superposition of stacked contours, where each patient instance is denoted with a distinct color, (ii) superposition of contour boxplots [WMK13], where each patient or cohort partition is denoted with a distinct color. The latter is shown in Figure 7 (a). A combination of the two is also possible, e.g., when comparing one patient instance to a specific partition. We additionally display the center point variations for each organ. These are explicitly encoded by drawing ellipsoid glyphs that deform in the direction of

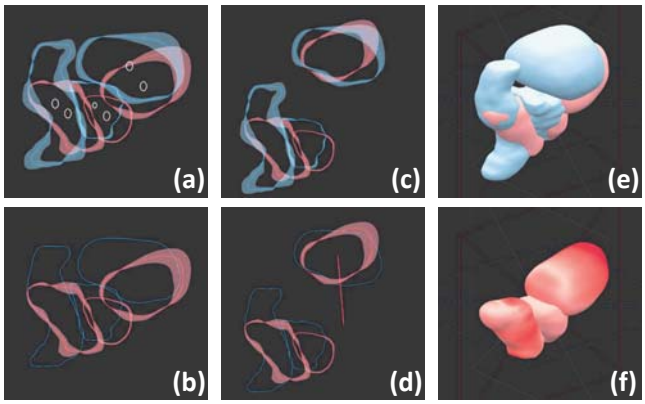

Figure 7: *Comparison of two partitions (red, blue) in the anatomical view.* ***(a)*** *Shape and positional variability are visible in 2D.* ***(b)*** *F+C on the red partition for shape variability. Positional variability has been hidden.* ***(c)*** *Exploded view for the extrusion of bladders in 2D.* ***(d)*** *F+C on the exploded bladder view with an indication of the extent of the extrusion.* ***(e)*** *Superposed 3D view.* ***(f)*** *Explicit encoding of variability in the 3D view for the red group only.*

the highest positional variance, to indicate the main directions in which the organs move, as shown in Figure 7 (a).

In the 3D views, we show the median shapes of all selected groups superimposed (Figure 7 (e)). The lighting in the scene and the surface material aim at highlighting the organ structure, while transparency is not employed. Instead, if a specific group is selected, it is brought forward with a F+C strategy in the 2D (Figure 7 (b)) and the 3D views. On demand, the 3D view can show the explicit encoding of the surface variations (Figure 7 (f)). In this case, the surface color is used to encode the amount of surface variation, using a sequential colormap based on the organs group color. With this view, we aim at supporting users trying to find regions with interesting shape changes. As the adjacency of the organs may cause overplotting and difficulties in judging the shape variations, we provide also an optional *exploded view* [BVG10], where the user can extrude the organs in the display (Figure 7 (c,d)). In this exploded view, the same organ of all groups is taken and placed in such a way that it does not overlap with any other shape, while at the same time being centered at a common point. To preserve parts of the initial context, a line glyph connects the center of the extruded organ to its original position (Figure 7 (d)).

Implementation: *Pelvis Runner* is designed as a server-client application. A webserver in conjunction with MATLAB performs the computationally expensive operations, including data processing, unraveling, and dimensionality reduction. A client-side browser application written in JavaScript receives the shape information and creates the visualizations using three.js and D3.js.

5. Results

In this section, we present four scenarios with single and multiple patients and organs and we evaluate how well tasks **(T1)** and **(T2)** are fulfilled, together with two domain experts (medical physicists). We further document the feedback of the two domain

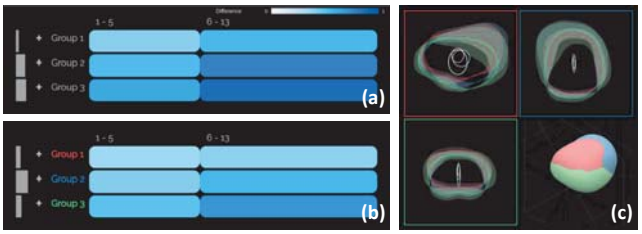

Figure 8: *Scenario (1)–Single Organ Cohort Exploration, showing the shape and positional variability of bladders.*

experts giving an initial indication of the strengths and weaknesses of the *Pelvis Runner*, and future improvements of our approach.

Scenario (1)–Single Organ Cohort Exploration: This scenario is depicted in Figure 8. We perform a grouping of patients based on their average bladder variability. When comparing each shape to the mean of the first treatment day (Figure 8 (a)), the bladder changes significantly through the treatment period. This is important, as normally only the first timestep is used for the treatment planning. When comparing each shape to the mean of the first five treatment days (Figure 8 (b)), the variability is lower. This can be an indication that performing the planning based on the first five timesteps instead of only the first one could more precisely model the shape of the bladder over time. The users can also explore the precise shape variations, as seen in the contour boxplots of Figure 8 (c). All groups have a similar shape, which can be due to the fact that patients with varying average variability are found all over the shape space and have no individually distinctive shape. The group with low shape variability (Group 1, red) has also small local shape variations and the group with high shape variability (Group 2, green) has also large local shape variations. The positional variations also correspond to the respective groups, the higher the general shape variability the larger the positional variations are. They also seem to largely vary along the sagittal axis (up–down), which corresponds to the findings of other works in this field [CMMH*17].

Scenario (2)–Multiple Organs Cohort Exploration: This scenario is depicted in Figure 9. The previous explorative tasks of Scenario (1) can be repeated for all organs present in the data. The cohort overview encodes the average values of the three organs side-by-side (Figure 9 (a)) or the deviation and missing value proportion for each organ in Figure 9 (b). The prostate (rightmost glyph) does not undergo any large shape variations, as it has low values (almost white) for all groups (Figure 9 (a)). This is due to the fact that prostate and CTV delineations are often used as the target area for the radiation treatment and are, therefore, not adapted in shape—only moved in position, even if their physical counterparts change. In Figure 9 (b), the coloring shows that the values for the bladders are rather similar in each group, while the ones of the rectum are strongly varying. The glyphs also reveal that around a third up to a half of all patients are missing a segmented prostate. Looking at the resulting contour variability plots in Figure 9 (c), the previous findings are confirmed in the anatomic view. Also, there are slight overlaps between the prostate shape and the bladder, which may result from the fact that the prostate shape includes an additional safety margin for adequate treatment. Also, all organs seem to un-

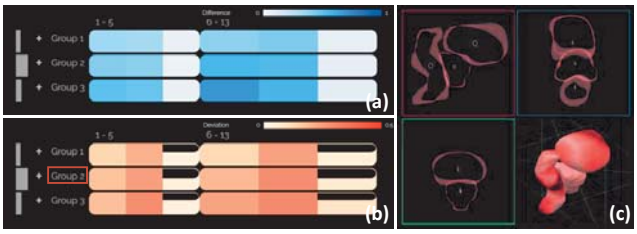

Figure 9: *Scenario (2)–Multiple Organs Cohort Exploration, showing the shape and positional variability of all pelvic organs.*

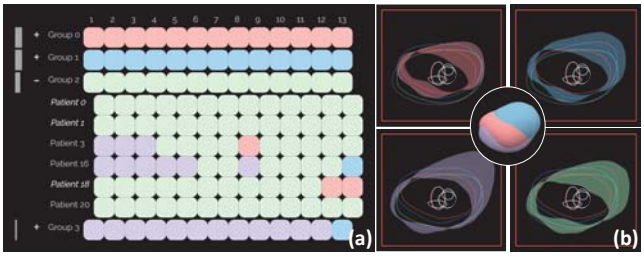

Figure 10: *Scenario (3)–Shape Type Identification, for bladder shape analysis.*

dergo the same positional changes, although the prostate seems to move slightly less—probably, due to anatomical confinement.

Scenario (3)–Shape Type Identification: This scenario is depicted in Figure 10, and it investigates possible organ shape types resulting from the clustering. In the case of the bladder, four groups (Figure 10 (a): red, green, blue, and purple) are obtained. Each group is selected to inspect their median shapes, confidence bands, and positions. The shapes produced in this scenario appear more different in form than the ones produced by splitting the shapes based on their average shape variation, as seen in the first two scenarios (Figure 10 (b)). Group 2 (green) and 3 (purple) are slightly bigger, and Group 2 bladders are more convex and protrude further in the direction of the prostate bottom left side of the shapes in Figure 10 (b)). This is not only visible in the 2D views but also in the superimposed 3D view. Both Group 0 (red) and 1 (blue) have a flatter interface towards the prostate (bottom left side of the shapes in Figure 10 (b)) and have a more concave shape. In general, all bladders tend to have the largest growth on the upper side, as this is the space where the bladder has the fewest constraints in the body and can freely extend. All of the bladders move predominantly along the sagittal axis (up–down), with Group 0 (red) and 3 (purple) moving more towards this direction. This verifies findings of previous clinical work [PAG*06, CMMH*17].

Scenario (4)–Retrospective Toxicity Analysis: This scenario is depicted in Figure 11, and investigates possible correlations of organ shapes to toxicity manifestation. This figure also showcases the comprehensive interface of the *Pelvis Runner*. For the toxicity, retrospective data of all patients are available. The elements are sorted based on this attribute, as seen in Figure 11 (a). Group 1 (red) presented no toxicity and Group 2 (blue) presented toxicity. In group 2, there are patients with high (1, 10 and 18) and low (0, 4) shape changes. Also there are patients whose average shape of the first five days is similar to the rest of the treatment (0, 1 and 14), and those whose average shape is not (10 and 18), leading to higher

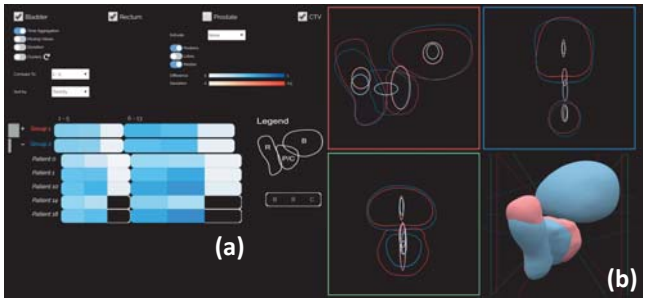

Figure 11: *Scenario (4)–Retrospective Toxicity Analysis, to compare patients with toxicity (blue) against patients without (red).*

variations. Both of these findings do not indicate a connection between bladder variability and induced toxicity. When looking at the anatomical views, there are no large differences in the shapes themselves, although the one with toxicity seems to be slightly bigger (Figure 11 (b)). However, the positional differences of the CTV look vastly different for the two groups of patients. Looking at the sagittal view (top left in Figure 11 (b)) indicates that the group with toxicity (blue) seems to move more than the one without (red). Increasing the number of patients might allow clinical researchers in the future to derive more information about these initial findings.

Initial Feedback: The domain experts also gave us feedback with regard to the strengths, weaknesses, limitations, and future improvements of our work. The domain experts commented that the application provides a flexible and systematic way to explore the data—allowing them to aggregate information in different ways and inspecting the most interesting aspects of these. The approach is "*a promising and useful decision-making tool for radiation oncologists*". As they stated, "*there are many possibilities, and many features*" and this allows them to approach their data in many different ways. It allows them to see individual organs, multiple organs, multiple patients, and also subgroups of the cohort, at the same time. Although this was not intended functionality, they commented that "*the tool offers a way of identifying the setup uncertainty of the entire treatment*", as it allows an overview of the motion, i.e., uncertainty, of the prostate. They also discussed that the ellipsoid glyph visualizing the positioning of the organs is more appropriate, as a probability distribution would show positions where the organ has never been. The exploded views of the organs were neither judged positively nor negatively—probably, due to their inherent distortion of the anatomy. The 2D views seemed to be more useful than the 3D views. The domain experts expressed that they would like to explore further the data in the frame of their future clinical research. They expect that working more with the application will bring forward interesting aspects for improvements—but most importantly, for the improvement of treatment planning. For example, the application could give "*indications of patients that will fail or that may develop toxicity at the beginning of the treatment*", allowing them to adapt the employed strategy. Potentially, it could help "*creating thresholds* [i.e., guidelines] *for patient treatment*". As points for future work, the domain experts proposed the addition of functionality for conducting easy annotations and measurements concerning, e.g., the confidence bands of the contour boxplots. This would quantify the up-to-now qualitative inspec-

tion of the variability, and could be done by, for example, probing along the median contour. Additionally, they would like to compare also the outcome of this approach with other applications, e.g., the *Bladder Runner* [RCMA*18]—or as they mentioned "*the two tools could be used in combination with each other and also with other metrics*". This is considered to be initial informal feedback, and in the future we would like to conduct an extensive evaluation.

6. Conclusions and Future Work

We present the *Pelvis Runner*, a visual analysis application for the exploration of segmented pelvic organs in multiple patients, across the whole radiation therapy treatment procedure. In this work, we focused on the global exploration and analysis of pelvic organ shape variability in an abstracted tabular view and on the local exploration and analysis in a combined 2D/3D anatomical view. We showcased the functionality of the *Pelvis Runner* with four usage scenarios conducted with two domain experts. Directions for future work include a thorough evaluation with the intended users, as well as a quantitative evaluation to assess the robustness of the current partitioning approach. For this, a larger cohort would also be needed. The registration part of the workflow could also be evaluated and improved to yield more robust results, as well as the chosen metrics for the shape space description. Additionally, potential occlusion issues in the anatomical view should be addressed. In its current state, the *Pelvis Runner* has been designed for domain experts—namely medical physicists—who are familiar with the implemented analysis and are also (up to a certain extent) visualization and machine learning literate. However, there is another group of potential users: clinicians, who are more involved into the design and administration of treatment plans. This group might significantly benefit from a simplified version of the application that focuses more on describing the organ shape variations of individual patients. Hereby, guidance [CGM*16] and a more automatized approach might be preferred. The *Pelvis Runner* is a first step towards the analysis of variability in multi-organ patient cohorts and its inclusion in adaptive radiotherapy.

Acknowledgments: This paper was partly written with the VRVis Competence Center, which is funded by BMVIT, BMDW, Styria, SFG and Vienna Business Agency in the scope of Competence Centers for Excellent Technologies (854174), managed by FFG.

References

[AHN*17] ALEMZADEH S., HIELSCHER T., NIEMANN U., CIBULSKI L., ITTERMANN T., VÖLZKE H., SPILIOPOULOU M., PREIM B.: Subpopulation Discovery and Validation in Epidemiological Data. In *EuroVis Workshop on Visual Analytics (EuroVA)* (2017), The Eurographics Association. 3

[BBF*11] BUSKING S., BOTHA C. P., FERRARINI L., MILLES J., POST F. H.: Image-based rendering of intersecting surfaces for dynamic comparative visualization. *The visual computer 27*, 5 (2011), 347–363. 3

[BBP10] BUSKING S., BOTHA C. P., POST F. H.: Dynamic multi-view exploration of shape spaces. In *Computer Graphics Forum* (2010), vol. 29, Wiley Online Library, pp. 973–982. 3

[BBS*18] BLUMENSCHEIN M., BEHRISCH M., SCHMID S., BUTSCHER S., WAHL D. R., VILLINGER K., RENNER B., REITERER H., KEIM D. A.: Smartexplore: Simplifying high-dimensional data analysis through a table-based visual analytics approach. In *IEEE Conference on Visual Analytics Science and Technology (VAST) 2018* (2018). 3, 5

[BCS96] BUJA A., COOK D., SWAYNE D. F.: Interactive high-dimensional data visualization. *Journal of computational and graphical statistics 5*, 1 (1996), 78–99. 6

[BSM*15] BERNARD J., SESSLER D., MAY T., SCHLOMM T., PEHRKE D., KOHLHAMMER J.: A visual-interactive system for prostate cancer cohort analysis. *Computer Graphics and Applications (CG&A), IEEE 35*, 3 (2015), 44–55. 3

[BVG10] BALABANIAN J.-P., VIOLA I., GRÖLLER M. E.: Interactive illustrative visualization of hierarchical volume data. *Proceedings of Graphics Interface 2010* (June 2010), 137–144. 7

[CGM*16] CENEDA D., GSCHWANDTNER T., MAY T., MIKSCH S., SCHULZ H.-J., STREIT M., TOMINSKI C.: Characterizing guidance in visual analytics. *IEEE Transactions on Visualization and Computer Graphics 23*, 1 (2016), 111–120. 9

[CM02] COMANICIU D., MEER P.: Mean shift: A robust approach toward feature space analysis. *IEEE Transactions on Pattern Analysis & Machine Intelligence*, 5 (2002), 603–619. 3

[CMMH*17] CASARES-MAGAZ O., MOISEENKO V., HOPPER A., PETTERSSON N. J., THOR M., KNOPP R., DEASY J. O., MUREN L. P., EINCK J.: Associations between volume changes and spatial dose metrics for the urinary bladder during local versus pelvic irradiation for prostate cancer. *Acta Oncologica 56*, 6 (2017), 884–890. 1, 2, 3, 7, 8

[CMRP*19] CASARES-MAGAZ O., RAIDOU R., PETTERSSON N., MOISEENKO V., EINCK J., HOPPER A., KNOPP R., MUREN L.: Bladder changes during first week of RT for prostate cancer determine the risk of urinary toxicity. *European SocieTy for Radiation & Oncology (ESTRO) 38* (2019). 1, 2

[CvHHB12] CHAI X., VAN HERK M., HULSHOF M. C., BEL A.: A voxel-based finite element model for the prediction of bladder deformation. *Medical physics 39*, 1 (2012), 55–65. 1, 2

[CvHvdK*11] CHAI X., VAN HERK M., VAN DE KAMER J. B., HULSHOF M. C., REMEIJER P., LOTZ H. T., BEL A.: Finite element based bladder modeling for image-guided radiotherapy of bladder cancer. *Medical physics 38*, 1 (2011), 142–150. 1, 2

[DJFB05] DELANEY G., JACOB S., FEATHERSTONE C., BARTON M.: The role of radiotherapy in cancer treatment. *Cancer 104*, 6 (2005), 1129–1137. 1

[ELL01] EVERITT B., LANDAU S., LEESE M.: Cluster analysis. *A member of the Hodder Headline Group, London* (2001), 429–438. 5

[FBW16] FERSTL F., BÜRGER K., WESTERMANN R.: Streamline variability plots for characterizing the uncertainty in vector field ensembles. *IEEE Transactions on Visualization and Computer Graphics 22*, 1 (2016), 767–776. 3, 6

[FGS*17] FURMANOVA K., GRATZL S., STITZ H., ZICHNER T., JARESOVA M., ENNEMOSER M., LEX A., STREIT M.: Taggle: Scalable visualization of tabular data through aggregation. *arXiv preprint arXiv:1712.05944* (2017). 6

[FKRW16] FERSTL F., KANZLER M., RAUTENHAUS M., WESTERMANN R.: Visual analysis of spatial variability and global correlations in ensembles of iso-contours. In *Computer Graphics Forum* (2016), vol. 35, Wiley Online Library, pp. 221–230. 3, 4, 6

[FKRW17] FERSTL F., KANZLER M., RAUTENHAUS M., WESTERMANN R.: Time-hierarchical clustering and visualization of weather forecast ensembles. *IEEE Transactions on Visualization and Computer Graphics 23*, 1 (2017), 831–840. 3

[HB03] HARROWER M., BREWER C. A.: Colorbrewer. org: an online tool for selecting colour schemes for maps. *The Cartographic Journal 40*, 1 (2003), 27–37. 5, 6

[Hil35] HILBERT D.: Über die stetige Abbildung einer Linie auf ein Flächenstück. In *Dritter Band: Analysis· Grundlagen der Mathematik· Physik Verschiedenes*. Springer, 1935, pp. 1–2. 4

[HK15] HERMANN M., KLEIN R.: A visual analytics perspective on shape analysis: state of the art and future prospects. *Computers & Graphics 53* (2015), 63–71. 3

[HSK11] HERMANN M., SCHUNKE A. C., KLEIN R.: Semantically steered visual analysis of highly detailed morphometric shape spaces. In *2011 IEEE Symposium on Biological Data Visualization (BioVis)*. (2011), IEEE, pp. 151–158. 3

[HSSK14] HERMANN M., SCHUNKE A. C., SCHULTZ T., KLEIN R.: A visual analytics approach to study anatomic covariation. In *2014 IEEE Pacific Visualization Symposium* (2014), IEEE, pp. 161–168. 3

[HSSK16] HERMANN M., SCHUNKE A. C., SCHULTZ T., KLEIN R.: Accurate interactive visualization of large deformations and variability in biomedical image ensembles. *IEEE Transactions on Visualization and Computer Graphics 22*, 1 (2016), 708–717. 3

[KCK17] KIM K., CARLIS J. V., KEEFE D. F.: Comparison techniques utilized in spatial 3d and 4d data visualizations: A survey and future directions. *Computers & Graphics 67* (2017), 138–147. 3, 6

[KERC09] KEEFE D., EWERT M., RIBARSKY W., CHANG R.: Interactive coordinated multiple-view visualization of biomechanical motion data. *IEEE Transactions on Visualization and Computer Graphics 15*, 6 (2009), 1383–1390. 3

[KFR03] KAZHDAN M., FUNKHOUSER T., RUSINKIEWICZ S.: Rotation invariant spherical harmonic representation of 3 d shape descriptors. In *Symposium on geometry processing* (2003), vol. 6, pp. 156–164. 3

[KLR*13] KLEMM P., LAWONN K., RAK M., PREIM B., TÖNNIES K. D., HEGENSCHEID K., VÖLZKE H., OELTZE S.: Visualization and analysis of lumbar spine canal variability in cohort study data. In *Vision, Modeling and Visualization* (2013), pp. 121–128. 3, 5

[KOJL*14] KLEMM P., OELTZE-JAFRA S., LAWONN K., HEGENSCHEID K., VÖLZKE H., PREIM B.: Interactive visual analysis of image-centric cohort study data. *IEEE Transactions on Visualization and Computer Graphics 20*, 12 (2014), 1673–1682. 3

[LvHB*05] LOTZ H. T., VAN HERK M., BETGEN A., POS F., LEBESQUE J. V., REMEIJER P.: Reproducibility of the bladder shape and bladder shape changes during filling. *Medical physics 32*, 8 (2005), 2590–2597. 1, 2

[MH08] MAATEN L. V. D., HINTON G.: Visualizing data using t-sne. *Journal of machine learning research 9*, Nov (2008), 2579–2605. 3, 5

[MLK*07] MOISEENKO V., LIU M., KRISTENSEN S., GELOWITZ G., BERTHELET E.: Effect of bladder filling on doses to prostate and organs at risk: a treatment planning study. *Journal of Applied Clinical Medical Physics 8*, 1 (2007), 55–68. 1

[MSD03] MUREN L. P., SMAALAND R., DAHL O.: Organ motion, set-up variation and treatment margins in radical radiotherapy of urinary bladder cancer. *Radiotherapy and Oncology 69*, 3 (2003), 291–304. 2

[MWK14] MIRZARGAR M., WHITAKER R. T., KIRBY R. M.: Curve boxplot: Generalization of boxplot for ensembles of curves. *IEEE Transactions on Visualization and Computer Graphics 20*, 12 (2014), 2654–2663. 3

[NDSM*19] NEJAD-DAVARANI S. P., SEVAK P., MONCION M., GARBARINO K., WEISS S., KIM J., SCHULTZ L., ELSHAIKH M. A., RENISCH S., GLIDE-HURST C.: Geometric and dosimetric impact of anatomical changes for mr-only radiation therapy for the prostate. *Journal of applied clinical medical physics* (2019). 2, 3

[PAG*06] PINKAWA M., ASADPOUR B., GAGEL B., PIROTH M. D., HOLY R., EBLE M. J.: Prostate position variability and dose–volume histograms in radiotherapy for prostate cancer with full and empty bladder. *International Journal of Radiation Oncology* Biology* Physics 64*, 3 (2006), 856–861. 8

[PI97] PEURA M., IIVARINEN J.: Efficiency of simple shape descriptors. *Aspects of visual form* (1997), 443–451. 3

[PKH*16] PREIM B., KLEMM P., HAUSER H., HEGENSCHEID K., OELTZE S., TOENNIES K., VÖLZKE H.: Visual analytics of image-centric cohort studies in epidemiology. In *Visualization in Medicine and Life Sciences III*. Springer, 2016, pp. 221–248. 3

[QLL*12] QUAN E. M., LI X., LI Y., WANG X., KUDCHADKER R. J., JOHNSON J. L., KUBAN D. A., LEE A. K., ZHANG X.: A comprehensive comparison of imrt and vmat plan quality for prostate cancer treatment. *International Journal of Radiation Oncology* Biology* Physics 83*, 4 (2012), 1169–1178. 2

[RBGR18] REITER O., BREEUWER M., GRÖLLER M., RAIDOU R.: Comparative visual analysis of pelvic organ segmentations. In *Proceedings of the Eurographics/IEEE VGTC Conference on Visualization: Short Papers* (2018), Eurographics Association, pp. 37–41. 3, 5

[RCMA*18] RAIDOU R. G., CASARES-MAGAZ O., AMIRKHANOV A., MOISEENKO V., MUREN L. P., EINCK J. P., VILANOVA A., GRÖLLER M.: Bladder runner: Visual analytics for the exploration of rt-induced bladder toxicity in a cohort study. In *Computer Graphics Forum* (2018), vol. 37, Wiley Online Library, pp. 205–216. 1, 2, 3, 5, 9

[RDCO*17] RIOS R., DE CREVOISIER R., OSPINA J. D., COMMANDEUR F., LAFOND C., SIMON A., HAIGRON P., ESPINOSA J., ACOSTA O.: Population model of bladder motion and deformation based on dominant eigenmodes and mixed-effects models in prostate cancer radiotherapy. *Medical image analysis 38* (2017), 133–149. 1, 2

[Shl14] SHLENS J.: A tutorial on principal component analysis. *arXiv preprint arXiv:1404.1100* (2014). 3, 5

[SMB*10] STEENWIJK M. D., MILLES J., BUCHEM M., REIBER J., BOTHA C. P.: Integrated visual analysis for heterogeneous datasets in cohort studies. In *IEEE VisWeek Workshop on Visual Analytics in Health Care* (2010), vol. 3, p. 3. 3

[SPA*14] SCHMIDT J., PREINER R., AUZINGER T., WIMMER M., GRÖLLER M. E., BRUCKNER S.: YMCA—Your mesh comparison application. In *2014 IEEE Conference on Visual Analytics Science and Technology (VAST)* (2014), IEEE, pp. 153–162. 4

[SRM*19] SCHLACHTER M., RAIDOU R., MUREN L., PREIM B., PUTORA P., BÜHLER K.: State-of-the-art report: Visual computing in radiation therapy planning. In *Computer Graphics Forum* (2019), vol. 38, Wiley Online Library. 2

[THLM*13] THARIAT J., HANNOUN-LEVI J.-M., MYINT A. S., VUONG T., GÉRARD J.-P.: Past, present, and future of radiotherapy for the benefit of patients. *Nature reviews Clinical oncology 10*, 1 (2013), 52. 1, 2

[TMA01] TORY M. K., MÖLLER T., ATKINS M. S.: Visualization of time-varying mri data for ms lesion analysis. In *Medical Imaging 2001: Visualization, Display, and Image-Guided Procedures* (2001), vol. 4319, International Society for Optics and Photonics, pp. 590–599. 4

[VLBK*13] VON LANDESBERGER T., BREMM S., KIRSCHNER M., WESARG S., KUIJPER A.: Visual analytics for model-based medical image segmentation: Opportunities and challenges. *Expert Systems with Applications 40*, 12 (2013), 4934–4943. 3

[VYM*10] VISWANATHAN A. N., YORKE E. D., MARKS L. B., EIFEL P. J., SHIPLEY W. U.: Radiation dose–volume effects of the urinary bladder. *International Journal of Radiation Oncology* Biology* Physics 76*, 3 (2010), S116–S122. 1, 2

[WFG*19] WEISSENBÖCK J., FRÖHLER B., GRÖLLER E., KASTNER J., HEINZL C.: Dynamic volume lines: Visual comparison of 3d volumes through space-filling curves. *IEEE Transactions on Visualization and Computer Graphics 25*, 1 (2019), 1040–1049. 5

[WHLS18] WANG J., HAZARIKA S., LI C., SHEN H.-W.: Visualization and visual analysis of ensemble data: A survey. *IEEE Transactions on Visualization and Computer Graphics* (2018). 3

[WL15] WASHINGTON C. M., LEAVER D. T.: *Principles and practice of radiation therapy*. Elsevier Health Sciences, 2015. 1, 2

[WMK13] WHITAKER R. T., MIRZARGAR M., KIRBY R. M.: Contour boxplots: A method for characterizing uncertainty in feature sets from simulation ensembles. *IEEE Transactions on Visualization and Computer Graphics 19*, 12 (2013), 2713–2722. 3, 4, 6